THE JOURNAL OF PHYSICAL CHEMISTRY LETTERS
A JOURNAL OF THE AMERICAN CHEMICAL SOCIETY

pubs.acs.org/JPCL Letter

^{15}N Hyperpolarization of Metronidazole Antibiotic in Aqueous Media Using Phase-Separated Signal Amplification by Reversible Exchange with Parahydrogen

Sergey V. Sviyazov, Dudari B. Burueva,* Nikita V. Chukanov, Ivan A. Razumov, Eduard Y. Chekmenev, Oleg G. Salnikov,* and Igor V. Koptyug

Cite This: *J. Phys. Chem. Lett.* 2024, 15, 5382−5389 Read Online

ABSTRACT: Metronidazole is a prospective hyperpolarized MRI contrast agent with potential hypoxia sensing utility for applications in cancer, stroke, neurodegenerative diseases, etc. We demonstrate a pilot procedure for production of ∼30 mM hyperpolarized [$^{15}N_3$]metronidazole in aqueous media by using a phase-separated SABRE-SHEATH hyperpolarization method, with nitrogen-15 polarization exceeding 2.2% on all three ^{15}N sites achieved in less than 2 min. The ^{15}N polarization T_1 of ∼12 min is reported for the $^{15}NO_2$ group at the clinically relevant field of 1.4 T in the aqueous phase, demonstrating a remarkably long lifetime of the hyperpolarized state. The produced aqueous solution of [$^{15}N_3$]metronidazole that contained only ∼100 μM of residual Ir was deemed biocompatible via validation through the MTT colorimetric test for assessing cell metabolic activity using human embryotic kidney HEK293T cells. This low-cost and ultrafast hyperpolarization procedure represents a major advance for the production of a biocompatible HP [$^{15}N_3$]-metronidazole (and potentially other hyperpolarized drugs) formulation for MRI sensing applications.

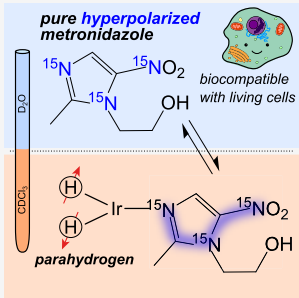

Among all diagnostic imaging modalities, magnetic resonance imaging (MRI) is of great importance for its ability of detecting structural abnormalities in organs without ionizing radiation exposure and excellent contrast in soft tissues.[1] Moreover, proton magnetic resonance spectroscopy (MRS) is a powerful noninvasive tool for detecting and mapping of metabolites with spatial resolution.[2] However, it is difficult to detect metabolic flux using this approach; thus, to study the active metabolism and its pathological alteration, modalities other than conventional proton MRS are needed. Heteronuclear MRS combined with administration of substrates labeled with stable and NMR-active isotopes (^{2}H, ^{13}C) allows unraveling of metabolic activity quantitatively.[3,4] In contrast to positron emission tomography (PET), MRS has the potential to reveal detailed metabolic information, since not only uptake can be monitored, but also the downstream labeled metabolites can be observed.[5] However, because of its intrinsically low sensitivity, heteronuclear MRS has been limited to relatively large voxel sizes, thus limiting its potential clinical utility.[6]

NMR hyperpolarization methods have recently emerged to circumvent the limitations posed by low NMR/MRI sensitivity. These approaches allow nuclear spins of contrast agents to be temporarily hyperpolarized; e.g., NMR signals are enhanced by 4−6 orders of magnitude at clinically relevant magnetic field strengths.[7−9]

To date, dissolution dynamic nuclear polarization (d-DNP)[10] is a widely utilized hyperpolarization approach: magnetic resonance imaging with hyperpolarized by means of d-DNP contrast agents enables noninvasive monitoring of metabolic processes in clinical studies.[11−13] Over 50 clinical trials with d-DNP are now in progress according to clinicaltrials.gov. While biomedical applications of parahydrogen-based hyperpolarization methods are only emerging,[14−18] they have already attracted significant attention because of their great potential for ultrafast and inexpensive production of hyperpolarized (HP) contrast agents. Parahydrogen (p-H_2; the spin isomer of molecular hydrogen with the total spin of 0) is a versatile source of hyperpolarization.[7] Parahydrogen-induced polarization (PHIP)[19] is based on the catalytic activation of p-H_2 with subsequent incorporation of p-H_2-derived protons into the hydrogenation product molecule. A more recent variant of the parahydrogen-based hyperpolarization approach does not require the hydrogenation step but generates signal amplification by reversible exchange (SABRE):[20] the substrate of interest and activated p-H_2 (in a form of hydride ligands) come into temporary contact on a metal complex (typically Ir),[21] allowing the spin polarization transfer from p-H_2-derived hydrides to the substrate nucleus to occur. The reversible exchange of both p-H_2 and substrate with

Received: March 24, 2024
Revised: May 2, 2024
Accepted: May 8, 2024
Published: May 13, 2024

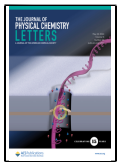

https://doi.org/10.1021/acs.jpclett.4c00875
J. Phys. Chem. Lett. 2024, 15, 5382−5389

their free counterparts in the solution leads to polarization buildup on the free substrate over multiple cycles of exchange. Depending on the experimental conditions, either protons or heteronuclei of interest in the substrate can be hyperpolarized in SABRE; direct hyperpolarization of heteronuclei (e.g., ^{13}C, ^{15}N) can be achieved at an ultralow magnetic field using the SABRE-SHEATH strategy (SABRE in Shield Enables Alignment Transfer to Heteronuclei).[22−25]

The range of molecules amenable to SABRE hyperpolarization is expanding rapidly.[26] While the leading sensing HP molecule is [1-^{13}C]pyruvate due to its central location in energy metabolic fluxes, HP nitroimidazole-based drugs have garnered considerable attention for potential biomedical sensing applications. Nitroimidazoles (metronidazole, nimorazole, ornidazole, etc.) are important antibacterial drugs acting on anaerobic infections. It is also known that nitroimidazoles are preferentially accumulated in O_2-starved tissues and thus are actively metabolized by anaerobic bacteria.[27] Accumulation of a reduced form of metronidazole and other structurally similar nitroimidazoles ultimately leads to selective cell death.[27] This property has been exploited widely in a number of biomedical applications beyond the antibiotic utility. For example, nitroimidazole-based derivatives can potentially serve as potent radiosensitizers for hypoxic tumors.[28] Similarly to anaerobic bacteria, cancerous tumors under hypoxic conditions selectively metabolize nitroimidazoles via irreversible reduction of the NO_2-group with the formation of reactive hydroxylamines which, in turn, bind with cellular macromolecules, causing cellular damage and making these cancer cells more amenable to therapy.[29] Moreover, pimonidazole (a representative member of the nitroimidazole family) staining is a marker of hypoxia and is routinely employed in immunohistochemistry.[30] Building on this success, nitroimidazole-based PET tracers have been developed to noninvasively image hypoxia in tumors, which is associated with more aggressive tumor phenotype and resistance to chemo- and radiation therapy.[31−33] These tracers (e.g., ^{18}F-labeled ^{18}F-fluoromisonidazole or FMISO[34]) have been deployed in cancer imaging.[34] The key limitation of FMISO PET imaging is the use of a radioactive tracer and very long scan time due to long clearance time (1−2 h) from the surrounding tissues. Since the ^{18}F half-life is 2 h, the long clearance time requires the use of higher radiation dose (as compared to other PET tracers), further dampening the clinical enthusiasm for this novel hypoxia imaging approach in deep tissue.

To address this limitation of nitroimidazole-based PET tracers for hypoxia imaging, the use of HP nitroimidazoles was proposed with the idea that the ^{15}N chemical shifts of HP nitroimidazole moiety can potentially report on the stepwise reduction process of this moiety in the hypoxic tissues, thus acting as a reporter of hypoxia.[35−42] Indeed, computational studies revealed the feasibility of employing HP uniformly ^{15}N-labeled metronidazole ([$^{15}N_3$]metronidazole) for hypoxia sensing applications.[43] Moreover, pilot ^{15}N d-DNP studies using HP [$^{15}N_3$]metronidazole revealed the feasibility of *in vivo* utilization of HP [$^{15}N_3$]metronidazole in healthy rats.[43] These developments make HP nitroimidazoles in general and HP [$^{15}N_3$]metronidazole in particular promising magnetic resonance sensors with diagnostic specificity to tumor hypoxia.[33]

It was shown previously that [$^{15}N_3$]metronidazole can be successfully hyperpolarized in deuterated methanol via SABRE-SHEATH with P_{15N} of ∼16% for the $^{15}NO_2$ group.[37] Despite this relatively high polarization level, it is imperative for *in vivo* MRI applications to produce a biocompatible HP bolus free from methanol and the cytotoxic SABRE catalyst.[44] Various purification strategies for SABRE-hyperpolarized agents are covered in the recent reviews.[45−47] These strategies include the use of aqueous media for the SABRE process using water-soluble catalysis,[48−51] capturing the catalyst,[52−54] the utilization of a perfluorinated biphasic system,[55] heterogeneous catalysis,[56−58] and others.[59] Here in this work we utilize an elegant approach recently proposed for generating a HP bolus in aqueous media while simultaneously achieving catalyst removal via phase transfer, dubbed "CASH-SABRE" or catalyst separated hyperpolarization through SABRE.[60]

The CASH-SABRE approach implies performing SABRE in a biphasic mixture, in which the substrate soluble in both phases is hyperpolarized in the organic phase ($CDCl_3$ or CD_2Cl_2) and then extracted into the aqueous phase (D_2O), while the SABRE catalyst, which is practically insoluble in water, remains in the organic phase. The schematic diagram of the process in presented in Figure 1. The ^1H nuclei of various

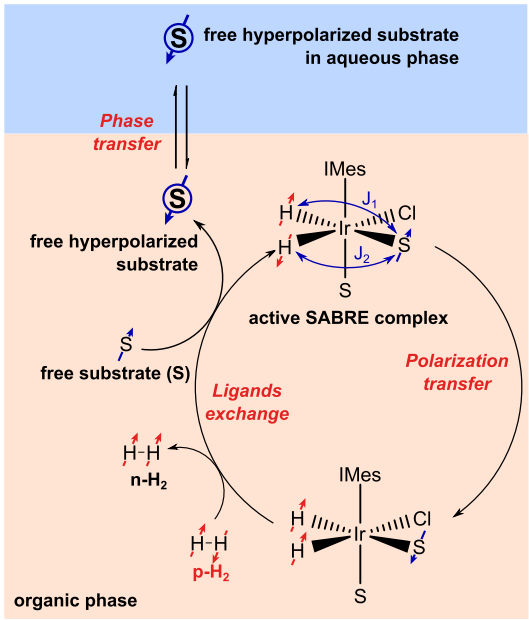

Figure 1. Scheme illustrating the CASH-SABRE approach. The SABRE catalyst resides predominantly in the organic phase, while the substrate can migrate between the two phases.

substrates were hyperpolarized using this approach, including pyrazine, 5-methylpyrimidine, methyl-4,6-d_2-nicotinate, 4,6-d_2-nicotinamide, and pyridazine; the obtained proton polarization levels were 2.5, 1.1, 9.7, 0.8, and 1.2% (per proton), respectively, after complete phase separation between D_2O and $CDCl_3$.[60] Moreover, it was shown that HP pyrazine can be obtained in aqueous solution with P_{13C} of 0.15% and P_{15N} of 0.98%.[60] The same approach was utilized for polarizing ornidazole at natural isotopic abundance: P_{15N} of ∼23% was observed for the N-3 site in the aqueous phase, while most of the SABRE catalyst was retained in CD_2Cl_2.[61] However, hyperpolarization of ^{13}C- and ^{15}N-enriched compounds was not demonstrated by this approach to date.

In this work we show that aqueous solutions of HP [$^{15}N_3$]metronidazole can be produced using catalyst separated hyperpolarization through the SABRE-SHEATH method. This hyperpolarization protocol produced P_{15N} exceeding 2.2% on

https://doi.org/10.1021/acs.jpclett.4c00875
J. Phys. Chem. Lett. 2024, 15, 5382−5389

all three ^{15}N sites. The biocompatibility of the resulting HP bolus is confirmed using the colorimetric cell proliferation assay (the MTT test) on human embryotic kidney HEK293T cells to demonstrate their viability in the presence of HP solution. The residual Ir concentration is 20 ± 2 μg/mL in the aqueous bolus, which corresponds to an Ir catalyst concentration of ∼100 ± 10 μM. The ∼52,000-fold ^{15}N NMR signal enhancement is achieved for the $^{15}NO_2$-group of [$^{15}N_3$]metronidazole at the clinically relevant field of 1.4 T in the aqueous phase. This inexpensive hyperpolarization procedure represents a major advance for potential application of [$^{15}N_3$]metronidazole as an HP contrast agent *in vitro/in vivo*.

For the CASH-SABRE experiment we first premixed 350 μL of D_2O containing 50 mM of [$^{15}N_3$]metronidazole (MNZ) and 350 μL of $CDCl_3$ containing 5 mM of SABRE precatalyst [Ir(IMes)(COD)Cl]. The resulting biphasic $CDCl_3/D_2O$ mixture (1:1 volume ratio) was placed in a 5 mm NMR tube tightly connected with a 1/4 in. o.d. PTFE tube. All experiments were carried out using a MATRESHCA hyperpolarizer.[62] It is worth mentioning that the hyperpolarizer was equipped with an additional presaturation chamber filled with $CDCl_3$ through which p-H_2 gas was supplied before bubbling through the sample chamber. This allowed us to compensate for the gradual evaporation of the volatile organic solvent and to maintain the long term stable operation under nearly constant experimental conditions and obtain reproducible results.[63] A schematic diagram of the experimental setup is presented in Figure S1 in the Supporting Information (SI). As metronidazole is soluble in both water and chloroform, for correct calculation of polarization levels the distribution of [$^{15}N_3$]metronidazole between the two phases was monitored for each data point from the ^1H NMR spectra at thermal equilibrium (see the SI for details). In order to acquire NMR spectra from a certain phase, the position of the NMR tube holder was precalibrated.

Both the precatalyst and the activated SABRE iridium complex were not noticeably dissolved in water, as during the experiment the aqueous phase remained colorless or only slightly colored (Figure S2). The SABRE precatalyst was activated via a continuous bubbling of p-H_2 gas through the $CDCl_3/D_2O$ mixture at a 20 standard cubic centimeters per minute (sccm) flow rate and 7.8 bar pressure. The activation was monitored using the SABRE-SHEATH procedure and the p-H_2 flow was interrupted only for the acquisition of ^{15}N NMR spectra (Figure S3). The ^{15}N NMR signals of hyperpolarized [$^{15}N_3$]MNZ in chloroform-*d* (both free and bound to the Ir center) reached a plateau after ∼20 min of activation. Further p-H_2 bubbling led to a partial chloroform-*d* evaporation. The polarization of [$^{15}N_3$]MNZ dissolved in D_2O reached the maximum levels after ∼2 h of activation, when the $CDCl_3/D_2O$ volume ratio approached 1:2. Thus, a typical CASH-SABRE solution represented the mixture of ∼350 μL of D_2O containing ∼32 mM of [$^{15}N_3$]MNZ and ∼175 μL of $CDCl_3$ containing ∼10 mM of the activated Ir complex and ∼16 mM of free [$^{15}N_3$]MNZ.

It is important to note that after activation the main form of Ir is a neutral [Ir(IMes)$(MNZ)_2(H)_2$Cl] complex, in which one of the two MNZ ligands and Cl occupy the equatorial positions, whereas another MNZ ligand is at the axial position (Figure 1). The hydrides are therefore chemically inequivalent and have ^1H chemical shifts of −23.9 and −25.3 ppm; the ^1H NMR spectrum of the hydride region at thermal equilibrium is presented in Figure S4. The rapid exchange of equatorial MNZ with its free counterpart in the solution results in the polarization buildup in the organic phase. Hyperpolarized [$^{15}N_3$]MNZ, in turn, is transferred to the aqueous phase. It should be mentioned that when the organic phase was removed and the remaining aqueous solution was exposed to the SABRE-SHEATH procedure, no enhanced ^{15}N NMR signals were observed, indicating low solubility of activated Ir complex in water. Biocompatibility of the produced HP bolus was further assessed via *in vitro* cytotoxicity and inductively coupled plasma atomic emission spectroscopy (ICP-AES) measurements, the results of which will be discussed below.

In this paper we show that [$^{15}N_3$]metronidazole at 32 mM concentration can be effectively hyperpolarized in aqueous media by the CASH-SABRE approach with the signal enhancement factors of 46,000−52,000 at the clinically relevant field of 1.4 T and P_{15N} of 2.5 ± 0.3%%, 2.2 ± 0.3%, and 2.3 ± 0.3% for $^{15}NO_2$, ^{15}N-3, and ^{15}N-1 sites, respectively. The spectra of hyperpolarized [$^{15}N_3$]MNZ are presented in Figure 2. For [$^{15}N_3$]MNZ dissolved in $CDCl_3$, the P_{15N} values

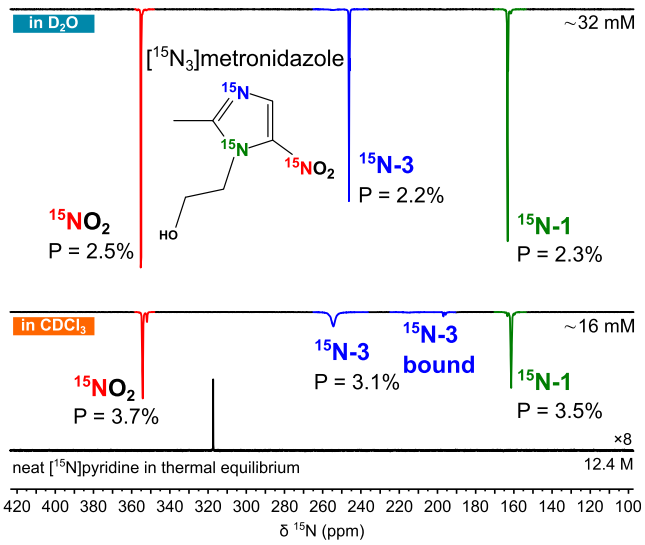

Figure 2. ^{15}N NMR spectra of [$^{15}N_3$]metronidazole hyperpolarized by SABRE-SHEATH acquired separately for the aqueous and the organic phases. The reference spectrum of thermally polarized neat [^{15}N]pyridine is presented at the bottom of the figure.

of 3.7 ± 0.4%, 3.1 ± 0.6%, and 3.5 ± 0.5% are observed for $^{15}NO_2$, ^{15}N-3, and ^{15}N-1 sites, respectively. Addition of salts (such as NaCl) can be beneficial for the phase separation; however, we did not observe any positive effect of NaCl (0.16 and 0.32 wt %) added to the $CDCl_3/D_2O$ mixture on the observed P_{15N} levels in the aqueous phase.

Studies of the polarization dynamics for [$^{15}N_3$]-metronidazole are summarized in Figure 3. In the CASH-SABRE experiment the supply of new portions of p-H_2 not only allows the polarization to accumulate, but also the presence of p-H_2 bubbles creates a gas−liquid−liquid interface, which therefore increases the interfacial area between two practically immiscible D_2O and $CDCl_3$ liquids. This, in turn, affects the efficiency of phase transfer of hyperpolarized [$^{15}N_3$]metronidazole from the organic to aqueous phase. It was observed that increasing the p-H_2 flow has a positive effect on the polarization levels (Figures 3a, 3b): in both phases the P_{15N} monotonously increases with the increase of p-H_2 flow

https://doi.org/10.1021/acs.jpclett.4c00875
J. Phys. Chem. Lett. 2024, 15, 5382−5389

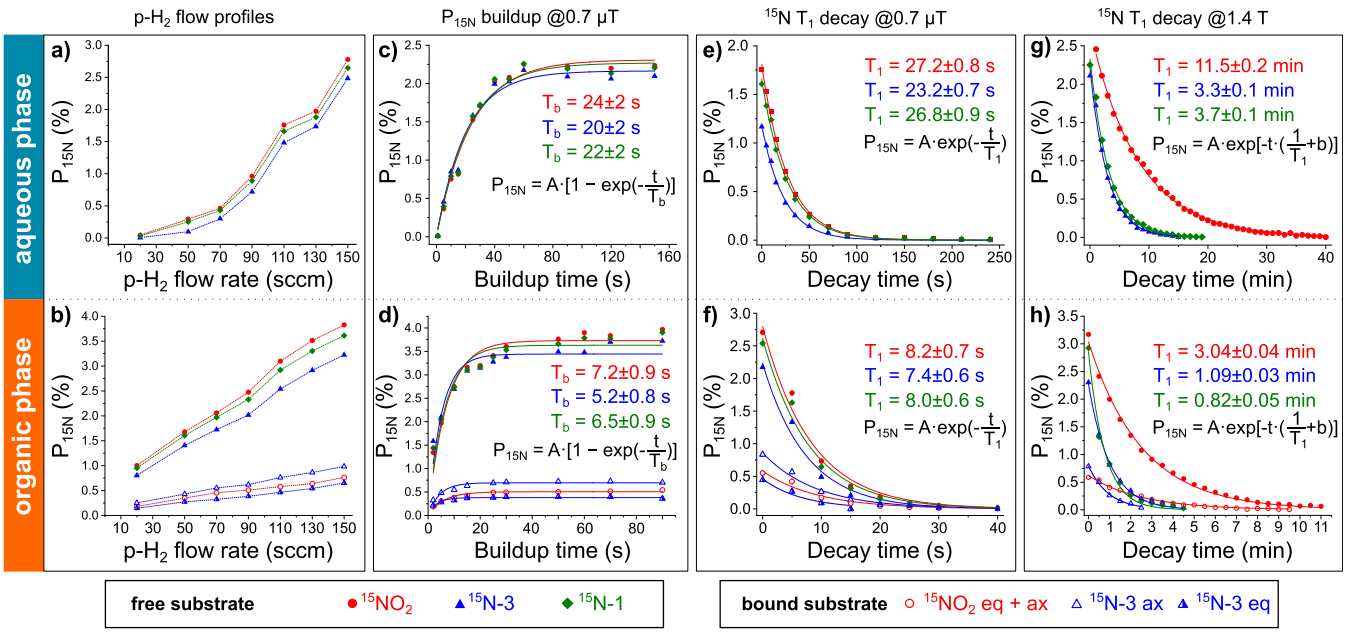

Figure 3. Hyperpolarization of [$^{15}N_3$]metronidazole in aqueous (top panel) and organic (bottom panel) phases achieved by the SABRE-SHEATH procedure after phase separation: (a−b) p-H_2 flow rate dependences of polarization of [$^{15}N_3$]MNZ. (c−d) P_{15N} buildup of [$^{15}N_3$]MNZ at 0.7 μT. (e−f) Relaxation decay of HP [$^{15}N_3$]MNZ at 0.7 μT. (g−h) Relaxation decay of HP [$^{15}N_3$]MNZ at 1.4 T. ^{15}N signal decay at 1.4 T was acquired using 15° flip-angle pulses applied every 30 s (panel h) or 1 min (panel g) to monitor the longitudinal relaxation time T_1 for [$^{15}N_3$]MNZ in the organic (h) or aqueous (g) phases. The corresponding equations used for the exponential fitting are presented for each experiment. For the aqueous phase only signals from free [$^{15}N_3$]MNZ were observed; in the organic phase the corresponding signals were observed for [$^{15}N_3$]MNZ bound to the Ir complex. All data were obtained at 23 °C, 7.8 bar p-H_2 pressure, and 150 sccm p-H_2 flow rate unless otherwise stated.

rate up to 150 sccm (which is a maximum flow rate allowed by the mass flow controller in our setup).

The ^1H-to-^{15}N polarization transfer was performed by p-H_2 bubbling at a constant ultralow magnetic field, in which the strong coupling regime is met. The magnetic field strength of ca. 0.7 μT was found to be optimal for [$^{15}N_3$]metronidazole, the details are described elsewhere.[42] The kinetics of ^{15}N polarization buildup at ca. 0.7 μT showed that the characteristic exponential buildup times T_b are similar for all three ^{15}N nuclei in the organic phase and are within the range of 5−7 s (Figure 3d); comparable buildup times were found for bound MNZ (Figure S5). For [$^{15}N_3$]MNZ in the aqueous phase the characteristic buildup times were significantly longer: T_b of 20−24 s was found for all three ^{15}N sites (Figure 3c).

The ultralow-field T_1 measurement was carried out by a series of manually controlled experiments where after polarizing the sample at the optimum transfer field (0.7 μT), the p-H_2 flow was interrupted and the sample was kept at 0.7 μT for a variable time before inserting it in a benchtop NMR spectrometer. A monoexponential fitting of the integrated signals yields approximately the same T_1 times of 7−8 s in the organic phase (Figure 3f) and 23−27 s in the aqueous phase (Figure 3e) for all three ^{15}N sites. These T_1 times are close to T_b values, indicating that polarization buildup is limited by relaxation at microtesla magnetic fields. The faster T_1 relaxation rates in chloroform compared to those in methanol reported elsewhere[42] can be attributed to the presence of an additional quadrupolar nucleus (^{35}Cl or ^{37}Cl) in the major iridium complex [Ir(IMes)$(MNZ)_2(H)_2$Cl] (it is known that coupling to quadrupolar nuclei significantly and negatively affects the attainable SABRE-SHEATH polarizations[40]).

To estimate ^{15}N T_1 relaxation times of [$^{15}N_3$]metronidazole at 1.4 T in both phases, 15° flip-angle pulses were used to excite the ^{15}N signals for acquisition once every 30 s (for T_1 measurement in the organic phase) or 1 min (for T_1 in the aqueous phase). The application of the small flip-angle pulse allowed the longitudinal relaxation times of all ^{15}N sites in [$^{15}N_3$]MNZ to be measured from the signal decay in just two experiments (one for each phase). The effective relaxation induced by the pulses (parameter $\frac{1}{b}$ in the equation, Figures 3g and 3h) corresponds to 14.42 min (Figure 3h) and 28.84 min (Figure 3g) for a 30 s and 1 min interval between spectral acquisitions, respectively (details on the calculations are given in the SI). An exponential fitting of the integrated signal yields a high-field (1.4 T) T_1 lifetime of the ^{15}N HP signals as follows: 11.5 ± 0.2 min for the $^{15}NO_2$ group, 3.3 ± 0.1 min for the ^{15}N-3 site, and 3.7 ± 0.1 min for the ^{15}N-1 site of [$^{15}N_3$]MNZ in the aqueous solution. [$^{15}N_3$]Metronidazole in the organic phase has significantly shorter ^{15}N T_1 relaxation times of 3.04 ± 0.04 min, 1.09 ± 0.03 min, and 0.82 ± 0.05 min for $^{15}NO_2$, ^{15}N-3, and ^{15}N-1, respectively. This significant difference between the relaxation times in different phases (as well as the similar difference in T_1 at 0.7 μT) clearly originates from the temporal association of [$^{15}N_3$]MNZ to the Ir complex in the organic phase. To the best of our knowledge, the ^{15}N T_1 relaxation time of ∼12 min is the longest observed for the $^{15}NO_2$-group of [$^{15}N_3$]MNZ at 1.4 T. Such an exceptionally long T_1 relaxation time would be useful for potential *in vivo* studies.

Next, the biocompatibility of the resulting aqueous HP bolus was assessed. First, an *in vitro* cells viability study was performed in a wide range of concentrations on a human embryonic kidney HEK293T cell line using an MTT test with 3 replicates of each concentration. 3-fold serial dilutions were prepared for solutions of interest in DMEM/F-12; the various bolus volumes (1.2, 3.7, 11.1, and 33.3%) were used for 1 h

https://doi.org/10.1021/acs.jpclett.4c00875
J. Phys. Chem. Lett. 2024, 15, 5382−5389

incubation. The results of the MTT test after 1 h incubation are presented in Figure 4. The cell viability was not

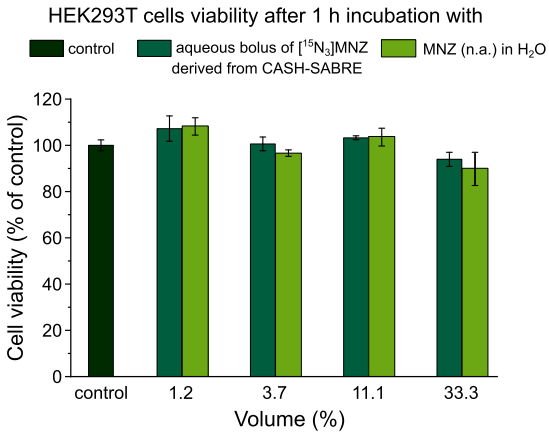

Figure 4. *In vitro* cells viability assessed by MTT test. Human embryonic kidney HEK293T cells were treated with an aqueous bolus of [$^{15}N_3$]metronidazole derived from CASH-SABRE for 1 h. The reference experiment was carried out for a solution of MNZ at natural isotopic abundance in H_2O (32 mM). The cell viability is presented as % of control. Data are the mean value of 3 independent experiments with a standard error.

significantly altered due to the 1 h exposure with the resulting aqueous solution of [$^{15}N_3$]MNZ derived from CASH-SABRE with the volume fractions of up to 33%. The cell viability is presented as % of control experiment, in which only DMEM/F12 was added without any other compounds. Besides, an additional experiment with an aqueous solution of commercially available metronidazole at natural isotopic abundance in H_2O with the same concentration (32 mM) was carried out. In such an experiment we deliberately eliminated the possible cytotoxic effects of both Ir and D_2O. However, we did not observe any statistically significant changes in the cell viability (Figure 4). The results of an MTT test with a longer exposure time (24 h) are presented in Figure S7. For comparison, the experiment with cisplatin injection (0.5 mg/mL) is presented as a positive control for cytotoxicity. No significant changes in the cell viability were observed for vol % values of up to 5% after the treatment with the aqueous [$^{15}N_3$]MNZ bolus. Both MTT assay results indicate that the Ir concentration in the aqueous bolus derived from CASH-SABRE is relatively low, since the activated Ir complex is known to have a pronounced cytotoxic effect.[44]

According to the elemental analysis performed using ICP AES, the residual Ir content was found to be 20 ± 2 μg/mL in the aqueous bolus, which corresponds to an Ir catalyst concentration of ∼100 ± 10 μM. Here in this work, we show ∼100-fold reduction of Ir concentration, from 10 mM to 100 μM. In another study with pyruvate hyperpolarization, a similar purification efficiency was achieved: the solvent evaporation followed by the Ir complex crystals filtration and subsequent dissolution in aqueous media resulted in the residual Ir concentration of 44 μM.[59]

Moreover, prior to the *in vivo*/*in vitro* administration, the HP bolus is typically diluted with saline or cell media, so in the final bolus the Ir concentration is expected to be 33−50 μM depending on the dilution ratio. In the previous study of catalyst separated SABRE of pyrazine, the upper limit of 1.5 μM on the residual Ir concentration in the aqueous phase was reported.[60] We associate such a difference with the fact that the efficiency of Ir catalyst separation depends on the substrate used in CASH-SABRE, since it affects the solubility of the activated Ir complex in water. However, it is important to note that 1.5 μM is a rough estimation derived from the analysis of UV−vis spectra for both phases. The absence of the absorbance line corresponding to the activated Ir complex in $CDCl_3$ in the UV−vis spectra from the aqueous phase was a sign of low Ir concentration; however, Ir can be present in $CDCl_3$ and D_2O in different complexes with different absorbance properties.

It is known that chloroform is partially soluble in water; however, the chloroform-*d* concentration in the produced aqueous solutions was not monitored. As was discussed in ref 60, N_2 purging can be beneficial to lower chloroform-*d* concentration, as well as the use of a lipophilic resin for the final purification can be adapted from the PHIP-SAH method.[64] Moreover, the subsequent purification via Ir scavenging using functionalized silicas[52−54] to levels permitted for *in vivo* administration is envisioned. We expect that the automation and setup optimization can be performed to further improve the efficiency of the CASH-SABRE procedure to reach even better polarization values. Moreover, the ^{15}N relaxation in sub-microtesla fields is very unfavorable, and performing such experiments using recently developed pulsed-SABRE-SHEATH approaches, which employ higher fields with substantially more favorable T_1 values, may also prove instrumental to further improve the polarization efficiency—indeed, we envision that creating P_{15N} over 20% may be feasible in the near future (work in progress in our laboratories[14,65]).

In conclusion, we have demonstrated the ^{15}N SABRE-SHEATH hyperpolarization of [$^{15}N_3$]metronidazole in aqueous media. SABRE-SHEATH in the biphasic mixture of $CDCl_3$ and D_2O (1:2 volume ratio) enabled the P_{15N} values of 2.5 ± 0.3%, 2.2 ± 0.3%, and 2.3 ± 0.3% for $^{15}NO_2$, ^{15}N-3, and ^{15}N-1 sites, respectively, for 32 mM [$^{15}N_3$]metronidazole in D_2O. The characteristic ^{15}N polarization T_1 is 12 min reported for the $^{15}NO_2$ group at a clinically relevant magnetic field of 1.4 T, demonstrating that the useable lifetime of HP bolus is tens of minutes—a remarkably long time window in the field of HP media. The approach proposed in this work was optimized to produce aqueous solutions of strongly polarized [$^{15}N_3$]-metronidazole accompanied by efficient Ir catalyst separation. The MTT test on human embryotic kidney HEK293T cells demonstrated the biocompatibility of the resulting aqueous HP bolus. The residual Ir concentration of 100 ± 10 μM was estimated using inductively coupled plasma atomic emission spectroscopy. This work paves the way for studies of nitroimidazoles metabolism *in vitro* and *in vivo* using hyperpolarized magnetic resonance technologies.

■ ASSOCIATED CONTENT

Supporting Information

The Supporting Information is available free of charge at https://pubs.acs.org/doi/10.1021/acs.jpclett.4c00875.

Experimental methods; polarization calculation procedures; schematic of experimental setup; photographs of the CASH-SABRE solution before and after the activation; SABRE-SHEATH activation curves; NMR spectra and plots; SABRE-SHEATH ^{15}N polarization buildup and decay for bound substrate; lifetime of the

https://doi.org/10.1021/acs.jpclett.4c00875
J. Phys. Chem. Lett. 2024, 15, 5382−5389

SABRE complex; and *in vitro* cells viability after 24 h of incubation (PDF)

AUTHOR INFORMATION

Corresponding Authors

Dudari B. Burueva − *International Tomography Center SB RAS, Novosibirsk 630090, Russia;* orcid.org/0000-0002-6077-5487; Email: burueva@tomo.nsc.ru

Oleg G. Salnikov − *International Tomography Center SB RAS, Novosibirsk 630090, Russia;* orcid.org/0000-0003-2266-7335; Email: salnikov@tomo.nsc.ru

Authors

Sergey V. Sviyazov − *International Tomography Center SB RAS, Novosibirsk 630090, Russia; Novosibirsk State University, Novosibirsk 630090, Russia*

Nikita V. Chukanov − *International Tomography Center SB RAS, Novosibirsk 630090, Russia; Novosibirsk State University, Novosibirsk 630090, Russia*

Ivan A. Razumov − *Novosibirsk State University, Novosibirsk 630090, Russia; Institute of Cytology and Genetics SB RAS, Novosibirsk 630090, Russia*

Eduard Y. Chekmenev − *Department of Chemistry, Integrative Bio-sciences (Ibio), Karmanos Cancer Institute (KCI), Wayne State University, Detroit, Michigan 48202, United States;* orcid.org/0000-0002-8745-8801

Igor V. Koptyug − *International Tomography Center SB RAS, Novosibirsk 630090, Russia;* orcid.org/0000-0003-3480-7649

Complete contact information is available at: https://pubs.acs.org/10.1021/acs.jpclett.4c00875

Author Contributions

The manuscript was written through contributions of all authors. All authors have given approval to the final version of the manuscript.

Notes

The authors declare the following competing financial interest(s): E.Y.C. holds a stake of ownership in XeUS Technologies Ltd. and serves on the scientific advisory board of Visma Life Sciences LLC.

ACKNOWLEDGMENTS

S.V.S., D.B.B., N.V.C., I.A.R., and O.G.S. thank the Russian Science Foundation (grant 21-73-10105) for the support of conducting both CASH-SABRE and cytotoxicity experiments. E.Y.C. thanks NIH R21EB033872 and National Science Foundation grant (NSF) CHE-1904780. The content is solely the responsibility of the authors and does not necessarily represent the official views of the National Institutes of Health. The authors thank Gennadiy A. Kostin from Nikolaev Institute of Inorganic Chemistry SB RAS for help with the ICP-AES analysis.

REFERENCES

(1) Kransdorf, M. J.; Murphey, M. D. Radiologic Evaluation of Soft-Tissue Masses: A Current Perspective. *Am. J. Roentgenol.* **2000**, *175* (3), 575−587.

(2) Öz, G.; Alger, J. R.; Barker, P. B.; Bartha, R.; Bizzi, A.; Boesch, C.; Bolan, P. J.; Brindle, K. M.; Cudalbu, C.; Dinçer, A.; Dydak, U.; Emir, U. E.; Frahm, J.; Gilberto González, R.; Gruber, S.; Gruetter, R.; Gupta, R. K.; Heerschap, A.; Henning, A.; Hetherington, H. P.; Howe, F. A.; Hüppi, P. S.; Hurd, R. E.; Kantarci, K.; Klomp, D. W. J.; Kreis, R.; Kruiskamp, M. J.; Leach, M. O.; Lin, A. P.; Luijten, P. R.; Marjańska, M.; Maudsley, A. A.; Meyerhoff, D. J.; Mountford, C. E.; Nelson, S. J.; Pamir, N.; Pan, J. W.; Peet, A. C.; Poptani, H.; Poptani, H.; Posse, S.; Pouwels, P. J. W.; Ratai, E. M.; Ross, B. D.; Scheenen, T. W. J.; Schuster, C.; Smith, I. C. P.; Soher, B. J.; Tkáč, I.; Vigneron, D. B.; Kauppinen, R. A. Clinical Proton MR Spectroscopy in Central Nervous System Disorders. *Radiology* **2014**, *270* (3), 658−679.

(3) Rothman, D. L.; de Feyter, H. M.; de Graaf, R. A.; Mason, G. F.; Behar, K. L. ^{13}C MRS Studies of Neuroenergetics and Neurotransmitter Cycling in Humans. *NMR Biomed* **2011**, *24* (8), 943−957.

(4) Chen Ming Low, J.; Wright, A. J.; Hesse, F.; Cao, J.; Brindle, K. M. Metabolic Imaging with Deuterium Labeled Substrates. *Prog. Nucl. Magn. Reson. Spectrosc.* **2023**, *134−135*, 39−51.

(5) Brindle, K. M. Imaging Cancer Metabolism Using Magnetic Resonance. *npj Imaging* **2024**, *2*, 1 DOI: 10.1038/s44303-023-00004-0.

(6) Rothman, D. L.; Howseman, A. M.; Graham, G. D.; Petroff, O. A. C.; Lantos, G.; Fayad, P. B.; Brass, L. M.; Shulman, G. I.; Shulman, R. G.; Prichard, J. W. Localized Proton NMR Observation of [3-^{13}C] Lactate in Stroke after [1-^{13}C] Glucose Infusion. *Magn. Reson. Med.* **1991**, *21* (2), 302−307.

(7) Eills, J.; Budker, D.; Cavagnero, S.; Chekmenev, E. Y.; Elliott, S. J.; Jannin, S.; Lesage, A.; Matysik, J.; Meersmann, T.; Prisner, T.; Reimer, J. A.; Yang, H.; Koptyug, I. V. Spin Hyperpolarization in Modern Magnetic Resonance. *Chem. Rev.* **2023**, *123* (4), 1417−1551.

(8) Hövener, J.-B.; Pravdivtsev, A. N.; Kidd, B.; Bowers, C. R.; Glöggler, S.; Kovtunov, K. V.; Plaumann, M.; Katz-Brull, R.; Buckenmaier, K.; Jerschow, A.; Reineri, F.; Theis, T.; Shchepin, R. V.; Wagner, S.; Bhattacharya, P.; Zacharias, N. M.; Chekmenev, E. Y. Parahydrogen-Based Hyperpolarization for Biomedicine. *Angew. Chem., Int. Ed.* **2018**, *57* (35), 11140−11162.

(9) Kovtunov, K. V.; Pokochueva, E. V.; Salnikov, O. G.; Cousin, S. F.; Kurzbach, D.; Vuichoud, B.; Jannin, S.; Chekmenev, E. Y.; Goodson, B. M.; Barskiy, D. A.; Koptyug, I. V. Hyperpolarized NMR: d-DNP, PHIP, and SABRE. *Chem. - An Asian J.* **2018**, *13* (15), 1857−1871.

(10) Ardenkjær-Larsen, J. H.; Fridlund, B.; Gram, A.; Hansson, G.; Hansson, L.; Lerche, M. H.; Servin, R.; Thaning, M.; Golman, K.; Ardenkjaer-Larsen, J. H.; Fridlund, B.; Gram, A.; Hansson, G.; Hansson, L.; Lerche, M. H.; Servin, R.; Thaning, M.; Golman, K. Increase in Signal-to-Noise Ratio of > 10,000 Times in Liquid-State NMR. *Proc. Natl. Acad. Sci. U. S. A.* **2003**, *100* (18), 10158−10163.

(11) Kurhanewicz, J.; Vigneron, D. B.; Ardenkjær-Larsen, J. H.; Bankson, J. A.; Brindle, K.; Cunningham, C. H.; Gallagher, F. A.; Keshari, K. R.; Kjaer, A.; Laustsen, C.; Mankoff, D. A.; Merritt, M. E.; Nelson, S. J.; Pauly, J. M.; Lee, P.; Ronen, S.; Tyler, D. J.; Rajan, S. S.; Spielman, D. M.; Wald, L.; Zhang, X.; Malloy, C. R.; Rizi, R. Hyperpolarized ^{13}C MRI: Path to Clinical Translation in Oncology. *Neoplasia* **2019**, *21* (1), 1−16.

(12) Skinner, J. G.; Menichetti, L.; Flori, A.; Dost, A.; Schmidt, A. B.; Plaumann, M.; Gallagher, F. A.; Hövener, J. B. Metabolic and Molecular Imaging with Hyperpolarised Tracers. *Mol. Imaging Biol.* **2018**, *20* (6), 902−918.

(13) Nelson, S. J.; Kurhanewicz, J.; Vigneron, D. B.; Larson, P. E. Z.; Harzstark, A. L.; Ferrone, M.; Van Criekinge, M.; Chang, J. W.; Bok, R.; Park, I.; Reed, G.; Carvajal, L.; Small, E. J.; Munster, P.; Weinberg, V. K.; Ardenkjær-Larsen, J. H.; Chen, A. P.; Hurd, R. E.; Odegardstuen, L. I.; Robb, F. J.; Tropp, J.; Murray, J. A. Metabolic Imaging of Patients with Prostate Cancer Using Hyperpolarized [1-^{13}C]Pyruvate. *Sci. Transl. Med.* **2013**, *5* (198), No. 198ra108.

(14) de Maissin, H.; Groß, P. R.; Mohiuddin, O.; Weigt, M.; Nagel, L.; Herzog, M.; Wang, Z.; Willing, R.; Reichardt, W.; Pichotka, M.; Heß, L.; Reinheckel, T.; Jessen, H. J.; Zeiser, R.; Bock, M.; von Elverfeldt, D.; Zaitsev, M.; Korchak, S.; Glöggler, S.; Hövener, J.-B.; Chekmenev, E. Y.; Schilling, F.; Knecht, S.; Schmidt, A. B. In Vivo Metabolic Imaging of [1-^{13}C]Pyruvate-d$_3$ Hyperpolarized By Reversible Exchange With Parahydrogen. *Angew. Chem., Int. Ed.* **2023**, *62* (36), No. e202306654.

(15) Cavallari, E.; Carrera, C.; Sorge, M.; Bonne, G.; Muchir, A.; Aime, S.; Reineri, F. The ^{13}C Hyperpolarized Pyruvate Generated by ParaHydrogen Detects the Response of the Heart to Altered Metabolism in Real Time. *Sci. Rep.* **2018**, *8* (1), 8366.

(16) Stewart, N. J.; Nakano, H.; Sugai, S.; Tomohiro, M.; Kase, Y.; Uchio, Y.; Yamaguchi, T.; Matsuo, Y.; Naganuma, T.; Takeda, N.; Nishimura, I.; Hirata, H.; Hashimoto, T.; Matsumoto, S. Hyperpolarized ^{13}C Magnetic Resonance Imaging of Fumarate Metabolism by Parahydrogen-Induced Polarization: A Proof-of-Concept in Vivo Study. *ChemPhysChem* **2021**, *22* (10), 915−923.

(17) MacCulloch, K.; Browning, A.; Bedoya, D. G.; McBride, S. J.; Abdulmojeed, M. B.; Dedesma, C.; Goodson, B. M.; Rosen, M. S.; Chekmenev, E. Y.; Yen, Y.-F.; TomHon, P.; Theis, T. Facile Hyperpolarization Chemistry for Molecular Imaging and Metabolic Tracking of [1-^{13}C]Pyruvate in Vivo. *J. Magn. Reson. Open* **2023**, *16−17*, No. 100129.

(18) Hune, T. L. K.; Mamone, S.; Schmidt, A. B.; Mahú, I.; D'Apolito, N.; Wiedermann, D.; Brüning, J.; Glöggler, S. Hyperpolarized Multi-Organ Spectroscopy of Liver and Brain Using 1-^{13}C-Pyruvate Enhanced via Parahydrogen. *Appl. Magn. Reson.* **2023**, *54* (11−12), 1283−1295.

(19) Bowers, C. R.; Weitekamp, D. P. Parahydrogen and Synthesis Allow Dramatically Enhanced Nuclear Alignment. *J. Am. Chem. Soc.* **1987**, *109* (18), 5541−5542.

(20) Adams, R. W.; Aguilar, J. A.; Atkinson, K. D.; Cowley, M. J.; Elliott, P. I. P.; Duckett, S. B.; Green, G. G. R.; Khazal, I. G.; López-Serrano, J.; Williamson, D. C. Reversible Interactions with Para-Hydrogen Enhance NMR Sensitivity by Polarization Transfer. *Science* **2009**, *323* (5922), 1708−1711.

(21) Rayner, P. J.; Norcott, P.; Appleby, K. M.; Iali, W.; John, R. O.; Hart, S. J.; Whitwood, A. C.; Duckett, S. B. Fine-Tuning the Efficiency of Para-Hydrogen-Induced Hyperpolarization by Rational N-Heterocyclic Carbene Design. *Nat. Commun.* **2018**, *9* (1), 4251.

(22) Theis, T.; Truong, M. L.; Coffey, A. M.; Shchepin, R. V.; Waddell, K. W.; Shi, F.; Goodson, B. M.; Warren, W. S.; Chekmenev, E. Y. Microtesla SABRE Enables 10% Nitrogen-15 Nuclear Spin Polarization. *J. Am. Chem. Soc.* **2015**, *137* (4), 1404−1407.

(23) Truong, M. L.; Theis, T.; Coffey, A. M.; Shchepin, R. V.; Waddell, K. W.; Shi, F.; Goodson, B. M.; Warren, W. S.; Chekmenev, E. Y.; L. Truong, M.; Theis, T.; M. Coffey, A.; V. Shchepin, R.; W. Waddell, K.; Shi, F.; M. Goodson, B.; S. Warren, W.; Y. Chekmenev, E. ^{15}N Hyperpolarization by Reversible Exchange Using SABRE-SHEATH. *J. Phys. Chem. C* **2015**, *119* (16), 8786−8797.

(24) Barskiy, D. A.; Shchepin, R. V.; Coffey, A. M.; Theis, T.; Warren, W. S.; Goodson, B. M.; Chekmenev, E. Y. Over 20% ^{15}N Hyperpolarization in Under One Minute for Metronidazole, an Antibiotic and Hypoxia Probe. *J. Am. Chem. Soc.* **2016**, *138* (26), 8080−8083.

(25) Fekete, M.; Ahwal, F.; Duckett, S. B. Remarkable Levels of ^{15}N Polarization Delivered through SABRE into Unlabeled Pyridine, Pyrazine, or Metronidazole Enable Single Scan NMR Quantification at the MM Level. *J. Phys. Chem. B* **2020**, *124* (22), 4573−4580.

(26) Barskiy, D. A.; Knecht, S.; Yurkovskaya, A. V.; Ivanov, K. L. SABRE: Chemical Kinetics and Spin Dynamics of the Formation of Hyperpolarization. *Prog. Nucl. Magn. Reson. Spectrosc.* **2019**, *114−115*, 33−70.

(27) Dingsdag, S. A; Hunter, N. Metronidazole: An Update on Metabolism, Structure−Cytotoxicity and Resistance Mechanisms. *J. Antimicrob. Chemother.* **2018**, *73* (2), 265−279.

(28) Bonnet, M.; Hong, C. R.; Wong, W. W.; Liew, L. P.; Shome, A.; Wang, J.; Gu, Y.; Stevenson, R. J.; Qi, W.; Anderson, R. F.; Pruijn, F. B.; Wilson, W. R.; Jamieson, S. M. F.; Hicks, K. O.; Hay, M. P. Next-Generation Hypoxic Cell Radiosensitizers: Nitroimidazole Alkylsulfonamides. *J. Med. Chem.* **2018**, *61* (3), 1241−1254.

(29) Rashed, F. B.; Diaz-Dussan, D.; Mashayekhi, F.; Macdonald, D.; Nation, P. N.; Yang, X.-H.; Sokhi, S.; Stoica, A. C.; El-Saidi, H.; Ricardo, C.; Narain, R.; Ismail, I. H.; Wiebe, L. I.; Kumar, P.; Weinfeld, M. Cellular Mechanism of Action of 2-Nitroimidazoles as Hypoxia-Selective Therapeutic Agents. *Redox Biol.* **2022**, *52*, No. 102300.

(30) Ragnum, H. B.; Vlatkovic, L.; Lie, A. K.; Axcrona, K.; Julin, C. H.; Frikstad, K. M.; Hole, K. H.; Seierstad, T.; Lyng, H. The Tumour Hypoxia Marker Pimonidazole Reflects a Transcriptional Programme Associated with Aggressive Prostate Cancer. *Br. J. Cancer* **2015**, *112* (2), 382−390.

(31) Hendrickson, K.; Phillips, M.; Smith, W.; Peterson, L.; Krohn, K.; Rajendran, J. Hypoxia Imaging with [F-18] FMISO-PET in Head and Neck Cancer: Potential for Guiding Intensity Modulated Radiation Therapy in Overcoming Hypoxia-Induced Treatment Resistance. *Radiother. Oncol.* **2011**, *101* (3), 369−375.

(32) Cheng, J.; Lei, L.; Xu, J.; Sun, Y.; Zhang, Y.; Wang, X.; Pan, L.; Shao, Z.; Zhang, Y.; Liu, G. ^{18}F-Fluoromisonidazole PET/CT: A Potential Tool for Predicting Primary Endocrine Therapy Resistance in Breast Cancer. *J. Nucl. Med.* **2013**, *54* (3), 333−340.

(33) Kizaka-Kondoh, S.; Konse-Nagasawa, H. Significance of Nitroimidazole Compounds and Hypoxia-Inducible Factor-1 for Imaging Tumor Hypoxia. *Cancer Sci.* **2009**, *100* (8), 1366−1373.

(34) Masaki, Y.; Shimizu, Y.; Yoshioka, T.; Tanaka, Y.; Nishijima, K. I.; Zhao, S.; Higashino, K.; Sakamoto, S.; Numata, Y.; Yamaguchi, Y.; Tamaki, N.; Kuge, Y. The Accumulation Mechanism of the Hypoxia Imaging Probe "FMISO" by Imaging Mass Spectrometry: Possible Involvement of Low-Molecular Metabolites. *Sci. Reports 2015 51* **2015**, *5* (1), 1−9.

(35) Shchepin, R. V.; Jaigirdar, L.; Chekmenev, E. Y. Spin−Lattice Relaxation of Hyperpolarized Metronidazole in Signal Amplification by Reversible Exchange in Micro-Tesla Fields. *J. Phys. Chem. C* **2018**, *122* (9), 4984−4996.

(36) Ariyasingha, N. M.; Lindale, J. R.; Eriksson, S. L.; Clark, G. P.; Theis, T.; Shchepin, R. V.; Chukanov, N. V.; Kovtunov, K. V.; Koptyug, I. V.; Warren, W. S.; Chekmenev, E. Y. Quasi-Resonance Fluorine-19 Signal Amplification by Reversible Exchange. *J. Phys. Chem. Lett.* **2019**, *10* (15), 4229−4236.

(37) Shchepin, R. V.; Birchall, J. R.; Chukanov, N. V.; Kovtunov, K. V.; Koptyug, I. V.; Theis, T.; Warren, W. S.; Gelovani, J. G.; Goodson, B. M.; Shokouhi, S.; Rosen, M. S.; Yen, Y.-F.; Pham, W.; Chekmenev, E. Y. Hyperpolarizing Concentrated Metronidazole $^{15}NO_2$ Group over Six Chemical Bonds with More than 15% Polarization and a 20 minute Lifetime. *Chem. − A Eur. J.* **2019**, *25* (37), 8829−8836.

(38) Shchepin, R. V.; Jaigirdar, L.; Theis, T.; Warren, W. S.; Goodson, B. M.; Chekmenev, E. Y. Spin Relays Enable Efficient Long-Range Heteronuclear Signal Amplification by Reversible Exchange. *J. Phys. Chem. C* **2017**, *121* (51), 28425−28434.

(39) Salnikov, O. G.; Chukanov, N. V.; Svyatova, A.; Trofimov, I. A.; Kabir, M. S. H.; Gelovani, J. G.; Kovtunov, K. V.; Koptyug, I. V.; Chekmenev, E. Y. ^{15}N NMR Hyperpolarization of Radiosensitizing Antibiotic Nimorazole by Reversible Parahydrogen Exchange in Microtesla Magnetic Fields. *Angew. Chem., Int. Ed.* **2021**, *60* (5), 2406−2413.

(40) Birchall, J. R.; Kabir, M. S. H.; Salnikov, O. G.; Chukanov, N. V.; Svyatova, A.; Kovtunov, K. V.; Koptyug, I. V.; Gelovani, J. G.; Goodson, B. M.; Pham, W.; Chekmenev, E. Y. Quantifying the Effects of Quadrupolar Sinks via ^{15}N Relaxation Dynamics in Metronidazoles Hyperpolarized via SABRE-SHEATH. *Chem. Commun.* **2020**, *56* (64), 9098−9101.

(41) Chukanov, N. V.; Shchepin, R. V.; Joshi, S. M.; Kabir, M. S. H.; Salnikov, O. G.; Svyatova, A.; Koptyug, I. V.; Gelovani, J. G.; Chekmenev, E. Y. Synthetic Approaches for ^{15}N-Labeled Hyperpolarized Heterocyclic Molecular Imaging Agents for ^{15}N NMR Signal Amplification by Reversible Exchange in Microtesla Magnetic Fields. *Chem. − A Eur. J.* **2021**, *27* (38), 9727−9736.

(42) Yi, A. P.; Salnikov, O. G.; Burueva, D. B.; Chukanov, N. V.; Chekmenev, E. Y.; Koptyug, I. V. Solvent Effects in Hyperpolarization of ^{15}N Nuclei in [$^{15}N_3$]Metronidazole and [$^{15}N_3$]Nimorazole Antibiotics via SABRE-SHEATH. *ChemRxiv* **2024**, DOI: 10.26434/chemrxiv-2024-6pg8b.

(43) Guarin, D. O.; Joshi, S. M.; Samoilenko, A.; Kabir, M. S. H.; Hardy, E. E.; Takahashi, A. M.; Ardenkjær-Larsen, J. H.; Chekmenev,

E. Y.; Yen, Y. F. Development of Dissolution Dynamic Nuclear Polarization of [$^{15}N_3$]Metronidazole: A Clinically Approved Antibiotic. *Angew. Chem., Int. Ed.* **2023**, *62* (31), No. e202219181.

(44) Manoharan, A.; Rayner, P. J.; Iali, W.; Burns, M. J.; Perry, V. H.; Duckett, S. B. Achieving Biocompatible SABRE: An in Vitro Cytotoxicity Study. *ChemMedChem.* **2018**, *13* (4), 352−359.

(45) Rayner, P. J.; Duckett, S. B. Signal Amplification by Reversible Exchange (SABRE): From Discovery to Diagnosis. *Angew. Chem., Int. Ed.* **2018**, *57* (23), 6742−6753.

(46) Robertson, T. B. R.; Mewis, R. E. Perspective on the Hyperpolarisation Technique Signal Amplification by Reversible Exchange (SABRE) in NMR Spectroscopy and MR Imaging. *Annu. Rep. NMR Spectrosc.* **2018**, *93*, 145−212.

(47) Salnikov, O. G.; Burueva, D. B.; Skovpin, I. V.; Koptyug, I. V. Parahydrogen-Based NMR Signal Amplification by Reversible Exchange (SABRE): Recent Advances and Applications. *Mendeleev Commun.* **2023**, *33* (5), 583−596.

(48) Truong, M. L.; Shi, F.; He, P.; Yuan, B.; Plunkett, K. N.; Coffey, A. M.; Shchepin, R. V.; Barskiy, D. A.; Kovtunov, K. V.; Koptyug, I. V.; Waddell, K. W.; Goodson, B. M.; Chekmenev, E. Y. Irreversible Catalyst Activation Enables Hyperpolarization and Water Solubility for NMR Signal Amplification by Reversible Exchange. *J. Phys. Chem. B* **2014**, *118* (48), 13882−13889.

(49) Colell, J. F. P.; Emondts, M.; Logan, A. W. J.; Shen, K.; Bae, J.; Shchepin, R. V.; Ortiz, G. X.; Spannring, P.; Wang, Q.; Malcolmson, S. J.; Chekmenev, E. Y.; Feiters, M. C.; Rutjes, F. P. J. T.; Blümich, B.; Theis, T.; Warren, W. S. Direct Hyperpolarization of Nitrogen-15 in Aqueous Media with Parahydrogen in Reversible Exchange. *J. Am. Chem. Soc.* **2017**, *139* (23), 7761−7767.

(50) Lehmkuhl, S.; Emondts, M.; Schubert, L.; Spannring, P.; Klankermayer, J.; Blümich, B.; Schleker, P. P. M. Hyperpolarizing Water with Parahydrogen. *ChemPhysChem* **2017**, *18* (18), 2426−2429.

(51) Spannring, P.; Reile, I.; Emondts, M.; Schleker, P. P. M.; Hermkens, N. K. J.; van der Zwaluw, N. G. J.; van Weerdenburg, B. J. A.; Tinnemans, P.; Tessari, M.; Blümich, B.; Rutjes, F. P. J. T.; Feiters, M. C. A New Ir-NHC Catalyst for Signal Amplification by Reversible Exchange in D_2O. *Chem. − A Eur. J.* **2016**, *22* (27), 9277−9282.

(52) Kidd, B. E.; Gesiorski, J. L.; Gemeinhardt, M. E.; Shchepin, R. V.; Kovtunov, K. V.; Koptyug, I. V.; Chekmenev, E. Y.; Goodson, B. M. Facile Removal of Homogeneous SABRE Catalysts for Purifying Hyperpolarized Metronidazole, a Potential Hypoxia Sensor. *J. Phys. Chem. C* **2018**, *122*, 16848−16852.

(53) Barskiy, D. A.; Ke, L. A.; Li, X.; Stevenson, V.; Widarman, N.; Zhang, H.; Truxal, A.; Pines, A. Rapid Catalyst Capture Enables Metal-Free Para-Hydrogen-Based Hyperpolarized Contrast Agents. *J. Phys. Chem. Lett.* **2018**, *9* (11), 2721−2724.

(54) Robertson, T. B. R.; Clarke, L. J.; Mewis, R. E. Rapid SABRE Catalyst Scavenging Using Functionalized Silicas. *Molecules* **2022**, *27* (2), 332.

(55) Ettedgui, J.; Blackman, B.; Raju, N.; Kotler, S. A.; Chekmenev, E. Y.; Goodson, B. M.; Merkle, H.; Woodroofe, C. C.; LeClair, C. A.; Krishna, M. C.; Swenson, R. E. Perfluorinated Iridium Catalyst for Signal Amplification by Reversible Exchange Provides Metal-Free Aqueous Hyperpolarized [1-^{13}C]-Pyruvate. *J. Am. Chem. Soc.* **2024**, *146* (1), 946−953.

(56) Shi, F.; Coffey, A. M.; Waddell, K. W.; Chekmenev, E. Y.; Goodson, B. M. Heterogeneous Solution NMR Signal Amplification by Reversible Exchange. *Angew. Chem., Int. Ed.* **2014**, *53* (29), 7495−7498.

(57) Shi, F.; Coffey, A. M.; Waddell, K. W.; Chekmenev, E. Y.; Goodson, B. M. Nanoscale Catalysts for NMR Signal Enhancement by Reversible Exchange. *J. Phys. Chem. C* **2015**, *119* (13), 7525−7533.

(58) Kovtunov, K. V.; Kovtunova, L. M.; Gemeinhardt, M. E.; Bukhtiyarov, A. V.; Gesiorski, J.; Bukhtiyarov, V. I.; Chekmenev, E. Y.; Koptyug, I. V.; Goodson, B. M. Heterogeneous Microtesla SABRE Enhancement of ^{15}N NMR Signals. *Angew. Chem., Int. Ed.* **2017**, *56* (35), 10433−10437.

(59) Schmidt, A. B.; De Maissin, H.; Adelabu, I.; Nantogma, S.; Ettedgui, J.; Tomhon, P.; Goodson, B. M.; Theis, T.; Chekmenev, E. Y. Catalyst-Free Aqueous Hyperpolarized [1-^{13}C]Pyruvate Obtained by Re-Dissolution Signal Amplification by Reversible Exchange. *ACS Sensors* **2022**, *7* (11), 3430−3439.

(60) Iali, W.; Olaru, A. M.; Green, G. G. R.; Duckett, S. B. Achieving High Levels of NMR-Hyperpolarization in Aqueous Media With Minimal Catalyst Contamination Using SABRE. *Chem. - Eur. J.* **2017**, *23* (44), 10491−10495.

(61) Iali, W.; Moustafa, G. A. I.; Dagys, L.; Roy, S. S. ^{15}N Hyperpolarisation of the Antiprotozoal Drug Ornidazole by Signal Amplification By Reversible Exchange in Aqueous Medium. *Magn. Reson. Chem.* **2021**, *59* (12), 1199−1207.

(62) Nantogma, S.; Chowdhury, M. R. H.; Kabir, M. S. H.; Adelabu, I.; Joshi, S. M.; Samoilenko, A.; de Maissin, H.; Schmidt, A. B.; Nikolaou, P.; Chekmenev, Y. A.; Salnikov, O. G.; Chukanov, N. V.; Koptyug, I. V.; Goodson, B. M.; Chekmenev, E. Y. MATRESHCA: Microtesla Apparatus for Transfer of Resonance Enhancement of Spin Hyperpolarization via Chemical Exchange and Addition. *Anal. Chem.* **2024**, *96* (10), 4171−4179.

(63) Blanchard, J. W.; Ripka, B.; Suslick, B. A.; Gelevski, D.; Wu, T.; Münnemann, K.; Barskiy, D. A.; Budker, D. Towards Large-Scale Steady-State Enhanced Nuclear Magnetization with in Situ Detection. *Magn. Reson. Chem.* **2021**, *59* (12), 1208−1215.

(64) Bondar, O.; Cavallari, E.; Carrera, C.; Aime, S.; Reineri, F. Effect of the Hydrogenation Solvent in the PHIP-SAH Hyperpolarization of [1-^{13}C]Pyruvate. *Catal. Today* **2022**, *397−399*, 94−102.

(65) Schmidt, A. B.; Eills, J.; Dagys, L.; Gierse, M.; Keim, M.; Lucas, S.; Bock, M.; Schwartz, I.; Zaitsev, M.; Chekmenev, E. Y.; Knecht, S. Over 20% Carbon-13 Polarization of Perdeuterated Pyruvate Using Reversible Exchange with Parahydrogen and Spin-Lock Induced Crossing at 50 μT. *J. Phys. Chem. Lett.* **2023**, *14* (23), 5305−5309.

https://doi.org/10.1021/acs.jpclett.4c00875
J. Phys. Chem. Lett. 2024, 15, 5382−5389